Article

Role of *pnc*A gene mutations W68R and W68G in Pyrazinamide resistance†

Mansi Aggarwal[a #], Aditi Singh[b,c #], Sonam Grover[d], Bharati Pandey[e], Anchala Kumari[b,c] and Abhinav Grover[b*]

[a]Amity Institute of Biotechnology, Amity University, Sector-125, Noida (U.P.)- 201313

[b]School of Biotechnology, Jawaharlal Nehru University, New Delhi 110067, India

[c]Department of Biotechnology, TERI University, Vasant Kunj, New Delhi 110070, India

[d]Kusuma School of Biological Sciences, Indian Institute of Technology Delhi 110016, India

[e]Department of Biotechnology, Panjab University, Chandigarh 160014, India

[#]Mansi Aggarwal and Aditi Singh contributed equally to this work.

*Corresponding Author

Mobile: +91-8130738032; +91-9891812561

Office Tel: +91-11-26738728

Fax: +91-11-26702040

Email: abhinavgr@gmail.com, agrover@jnu.ac.in

†This article has been accepted for publication and undergone full peer review but has not been through the copyediting, typesetting, pagination and proofreading process, which may lead to differences between this version and the Version of Record. Please cite this article as doi: [10.1002/jcb.26420]

Received 14 July 2017; Revised 14 September 2017; Accepted 3 October 2017
Journal of Cellular Biochemistry

DOI 10.1002/jcb.26420

Abstract

Mycobacterium tuberculosis (Mtb) resistance towards anti-tuberculosis drugs is a widespread problem. Pyrazinamide (PZA) is a first line antitubercular drug that kills semi-dormant bacilli when converted into its activated form i.e. pyrazinoic acid (POA) by Pyrazinamidase (PZase) enzyme coded by *pnc*A gene. In this study, we conducted several analyses on native and mutant structures (W68R, W68G) of PZase before and after docking with the PZA drug to explore the molecular mechanism behind PZA resistance caused due to *pnc*A mutations. Structural changes caused by mutations were studied with respect to their effects on functionality of protein. Docking was performed to analyze the protein-drug binding and comparative analysis was done to observe how the mutations affect drug binding affinity and binding site on protein. Native PZase protein was observed to have the maximum binding affinity in terms of docking score as well as shape complementarity in comparison to the mutant forms. Molecular dynamics simulation analyses showed that mutation in the 68th residue of protein results in a structural change at its active site which further affects the biological function of protein i.e. conversion of PZA to POA. Mutations in the protein thereby led to PZA resistance in the bacterium due to the inefficient binding.

Keywords: *Mycobacterium tuberculosis*, docking, molecular dynamics simulation, pyrazinamidase, PZA resistance

Introduction

Among humans, Tuberculosis (TB) which, spreads by aerosols is one of the leading cause of infection related deaths. Tuberculosis (TB) manifests upon infection by its bacterial causative agent, *Mycobacterium tuberculosis* (Mtb) [Organization, 2015]. As on 2015, 10.4 million individuals were infected with TB which led to the death of 1.5 million individuals around the world. One of the major reasons for this alarming rise in spread of TB is due to the emergence of drug resistant strains [Stehr et al., 2015]. In 2015, > 4.7 million new cases of Multi drug-resistant tuberculosis (MDR-TB) were detected which, resulted in about 250000 deaths [Organization, 2016]. Moreover, 9.7% people with MDR-TB were reported to have Extensively drug-resistant tuberculosis (XDR-TB) [Organization, 2015]. This burgeoning phenomenon of antibiotic resistance is believed to be the result of several point mutations in specific key resistance genes [Chan et al., 2007]. Thereby there is an urgent need to combat this disease. The World Health Organization recommended protocol of treatment for new TB patients is DOTS (directly observed treatment, short-course), which is a six months course involving four first-line drugs; isoniazid, rifampin, pyrazinamide and ethambutol [Organization, 2015]. However, this therapy is marred by the poor efficacy of first line anti-tubercular drugs and high toxic side effects of second line drugs [Dooley et al., 2012]. It is due to the fact that Mtb is impervious to numerous anti-toxins produced by other bacteria due to the presence of highly hydrophobic cell envelope acting as a permeability barrier [Cole et al., 1998].

Pyrazinamide (PZA), a derivative of nicotinamide, has the unique ability to kill persistent bacilli which resides in the low pH environment of the host macrophages, hence reducing the period of chemotherapy [Gu et al., 2015; Mitchison, 1985]. Nicotinamide was reported to have activity against *Mycobacterium* in animal models by Chorine in 1945 [Ryan, 1993]. PZA was identified as an active analog of nicotinamide by direct testing on a mouse model of TB infection [Malone et al., 1952; McKenzie et al., 1948; Solotorovsky et al., 1952]. Its role as an anti-tuberculosis drug was discovered in 1952 [Yeager et al., 1952]. In 1996, it was confirmed that *pnc*A gene was strongly associated with intrinsic PZA resistance in Mtb [Scorpio and Zhang, 1996] and in 1997 it was found that mutations in *pnc*A gene constituted the significant reason behind PZA resistance [Scorpio and Zhang, 1996]. Pyrazinamidase (PZase) is a superfluous enzyme for the

survival of Mtb and henceforth puts no specific pressure on what type of mutations which occur. Hence a wide range of *pnc*A mutations are endured leading to high diversity of mutations in *pnc*A gene [Cheng et al., 2000]. These mutations result in amino acid substitution, insertion or deletion causing shift in the reading frame (Frameshift Mutations) that gives rise to abnormal, non-functional or prematurely terminated proteins [Lee et al., 2001; Scorpio et al., 1997].

PZA is a pro-drug which is toxic to bacteria when converted into its active form, pyrazinoic acid (POA). *pnc*A gene encodes PZase protein which catalyses the conversion of PZA into POA. PZase plays a crucial role in PZA drug action and is expressed in the cytoplasm [Chang et al., 2011]. PZA targets only the semi-dormant bacilli. Accumulation of POA has been shown to inhibit various functions in Mtb at a lower pH due to the deficient POA efflux mechanism. This causes destabilization of potential of the membrane, blocking the membrane transport function [Konno et al., 1967; Zhang et al., 2008; Zhang and Telenti, 2000]. *Mycobacterium smegmatis* is naturally impervious to PZA because of the presence of a dynamic POA efflux mechanism [Zhang et al., 1999]. PZA resistance is caused due to mutations in *pnc*A, *rps*A and *pan*D genes. Loss of PZase activity is associated with mutations in the *pnc*A gene [Bamaga et al., 2002]. This results in PZA resistance due to the non-synonymous mutations in the *pnc*A gene [Zhang and Mitchison, 2003]. RpsA is a target of PZA involved in the process of trans-translation. Mutations in the *rps*A gene prevents POA binding, thereby further inhibiting the trans-translation resulting in accumulation of toxic polypeptides and cell death under stress conditions [Shi et al., 2011]. Moreover, *pan*D encoding aspartate decarboxylase is involved in PZA resistance affecting the pantothenate biosynthetic pathway [Pandey et al., 2016; Zhang et al., 2013]. It is thereby vital to comprehend the phenomenon behind drug resistance by analyzing the 3D structure of the mutant proteins.

In this report, we have studied the PZase enzyme, having a 185 amino acid long chain, that consists of six parallel β-sheet having α-helices on both sides forming an α/β domain [Petrella et al., 2011]. The substrate binding cavity has a catalytic triad made from the residues Asp8, Lys96, and Cys138 before the termination of β-strand 3, β-strand 1 and at the N-terminal of α- helix 3, respectively. Opposite to the substrate binding cavity is the metal ion binding site which holds the Fe^{2+} ion. It is formed by the residues Asp49, His51, His57 and His71[Vats et al., 2015].

Besides Fe^{2+} ion, PZA also binds in the cavity. Some degree of clustering observed at three regions of PZase (3 to 17, 61 to 85, and 132 to 142). Mutations in these residues greatly affected the function of PZase [Du et al., 2001; Lemaitre et al., 1999; Petrella et al., 2011; Sheen et al., 2012].

The native PZase protein and mutant W68G and W68R PZase proteins were selected for this study. Various analyses were performed which included binding pocket determination, shape complementarity computation, receptor-ligand interaction, docking simulation and molecular dynamics (MD) simulations to comprehend the impact of genetic mutations on structure and function of the protein. MD simulations allowed the investigation of conformational changes that happened to the 3D structure of the protein due to mutations in the gene encoding it. They additionally helped to observe the dynamic conformational changes that occurred within the interactions between the ligand and protein [Purohit et al., 2011; Singh et al., 2017]. MD simulations for the native and mutant protein structures, solvated in water, were run for modeling the protein behavior and to assess the physical reason for drug resistance. The principle goal of this study was to comprehend the mechanism causing PZA resistance at molecular level in TB infected patients which, in turn would enable the development of robust and improved molecular diagnostic techniques. Moreover, the knowledge gained following this study, regarding the mechanism of resistance of PZA towards Mtb could help to develop prophylactic measures against the disease [Da Silva and Palomino, 2011].

Materials and methods

Data-set

We retrieved the structure of PncA protein (PDB ID 3PL1) [Petrella et al., 2011] from Protein Data Bank (PDB) [Berman et al., 2000]. The PDB native structure was also composed of a Fe^{2+} ion situated in the substrate binding cavity coordinated by one Aspartate residue and three Histidine residues. The crystallized water particles were excluded. The database did not had mutant structures and hence two point mutations were induced at 68^{th} position i.e. tryptophan to glycine and tryptophan to arginine in the native protein structure to obtain the mutant structures

using PyMOL [Schrödinger]. Also, the SMILES string of the drug PZA was retrieved from the PubChem database [Kim et al., 2015] maintained in NCBI. This was submitted to CORINA for construction of 3D structure of PZA. Energy minimization was done using GROMACS 5.0 package [Abraham et al., 2015] with all-atom OPLS force field for the protein structures.

Binding pocket determination

Binding cavity analysis was required to understand the protein-ligand interactions. We used computed atlas of surface topography of proteins (CASTp) algorithm [Dundas et al., 2006] for determining the binding pocket of native and mutant proteins. This algorithm used Delaunay triangulation, alpha shape and discrete flow for taking measurements. It distinguished and measured the pockets on surface and interior of the proteins. Following which, it calculated the volume and area for each cavity and pocket, either present on the surface accessible to the solvent (Richards' surface) or surface of the molecule (Connolly's surface). Probe radius of 1.4Å was set as default and the pockets detected were ranked with their volumes and area. We selected the pocket with maximum volume for analysis.

Shape complementarity computation

PatchDock [Duhovny et al., 2002; Schneidman-Duhovny et al., 2005] is a docking algorithm based on geometry for protein-protein and protein-ligand complexes. This algorithm comprehended the molecular shape representation of protein, surface patch matching, filtering and scoring. It discovered the docking transformations which yielded the best complementarities in molecular shape by initiating wide interface area and steric clashes which guaranteed that different coordinated components of docked molecules having complementary qualities are incorporated. The Connolly dot surface representation [Emekli et al., 2008] of molecules had various shape-based patches: convex, concave and flat surfaces. The patches were coordinated using Geometric Hashing and Pose-Clustering procedures to enhance the shape complementarity function. Concave patches were coordinated with convex patches whereas the flat patches were coordinated with either of the two to produce candidate transformations. These transformations were analyzed to discard the ones with unsatisfactory penetrations and RMSD clustering with default value of 4Å was used to discard the repetitive transformations as well. Every transformation assessed was based on the geometric fit of the complex along with its atomic

desolvation energy [Schneidman-Duhovny et al., 2005; Zhang et al., 1997]. A table was generated which gave the geometric score, desolvation energy, interface area and rigid transformation and the PDB file of the solution.

Receptor-ligand interaction

Receptor-ligand interaction was studied using the Glide module [Halgren et al., 2004] of Schrodinger [Glide, 2009], similar to the previous studies of our group [Jamal et al., 2016; Nagpal et al., 2015; Singh et al., 2016; Sinha et al., 2016]. In this study, we utilized the flexible ligand docking procedures. Schrodinger's protein preparation wizard was used to prepare the protein structure [Sastry et al., 2013; Schrödinger, 2013] where the hydrogen atoms were included, bond lengths were corrected, disulphide bonds were made, terminal residues capped and selenomethionines were changed into methionine [Friesner et al., 2004]**.** Ligand was also prepared using Schrodinger's LigPrep module [Release, 2013] which produced possible chiral, stereo chemical and ionization variations of PZA. Maximum 32 conformers were considered for PZA. A grid was generated using Schrodinger's Receptor grid generation application around the active site residues Cys138, Thr135, Ala134, Ile133, Lys96, His71, Trp68, Phe58, His57, His51, Asp49, Phe13 and Asp8 [Lakshmipathy et al., 2013; Unissa et al., 2011].

Extra precision docking protocol [Friesner et al., 2006] was implemented**.** Total ligand-receptor interaction energy was calculated on the basis of van der Waals interaction forces, electrostatic energy and H-bond interactions within the ligand and receptor. Electrostatic forces were made appropriate to understand how a molecule interacts with other molecules in its vicinity. Formation of H-bonds and van der Waals interactions depends on the integral surfaces which pack together and also correctly position the charged atoms to form electrostatic bonds. Consequently, these polar associations improve the overall stability of complex [Jones and Thornton, 1996].

Molecular dynamics simulation

MD simulation was run on all the complexes using GROMACS 5.0 software package[Berendsen et al., 1995; Hess et al., 2008; Van Der Spoel et al., 2005] and GROMOS-96 43A1 force field [van Gunsteren et al., 1996]. The topology of ligand was generated using PRODRG web server [SchuÈttelkopf and Van Aalten, 2004; Verma et al., 2016b]. Each complex was solvated in a

cubic box with 1.5nm box space using simple point charge (spc) water model [Wu et al., 2006]. Wild protein and drug complex had 17673 SPC water molecules whereas the mutant W68G and W68R complexes had 16951 and 17126 SPC water molecules, respectively in the cubic box. Sodium and chloride ions were added into the cubic box by genion tool in GROMACS to neutralize the systems. These ions replaced the water molecules which had maximum electrostatic potential. Energy minimization was done for 50,000 cycles using the steepest descent algorithm and terminated on reaching a maximum force of 1000 kJ mol^{-1} nm^{-1}. Equilibration was done in two steps, first using NVT ensemble at 300K and then NPT ensemble for 300K and 1 bar pressure, each for 100ps. Temperature coupling was done using Berendsen thermostat method [Berendsen et al., 1984] and pressure was maintained constant by Parrinello–Rahman barostat [Parrinello and Rahman, 1981]. Linear constraint solver (LINCS) algorithm [Hess et al., 1997] rectified all the bond lengths. Fast particle-mesh Ewald (PME) [Darden et al., 1993] electrostatics method computed all the long-range electrostatic interactions. Finally, the production MD simulations were carried out on each complex for 40,000ps. Various analyses included in the scripts of GROMACS 5.0 package were performed [Van Der Spoel et al., 2005]. Trajectory files were analyzed by root-mean square deviation (RMSD), root-mean square fluctuations (RMSF) and radius of gyration (Rg) values using GROMACS utilities. Number of H-bonds, solvent accessible surface area (SASA) and energies like kinetic energy, potential energy, total energy, coulomb energy and short range energies were also calculated. Graphs were generated using the obtained values for each parameter.

Principal Component Analysis

Principal component analysis (PCA) is a mass-weighted covariance matrix based mathematical method whichwas utilized for deliberately diminishing the dimensionality of complex system [Verma et al., 2016c]. PCA extracted the dominant and concerted motion of proteins during simulations which were relevant for its biological function [Amadei et al., 1993]. A list of eigenvectors along with their respective eigenvalues was obtained. Eigenvectors are known as the principal components and eigenvalues indicate the amount of dynamical fluctuations contributed by them. Covariance matrix was plotted and diagonalized to obtain information about the correlated motion of residues in native and mutant proteins. This was utilized to catch the degree of co-linearity for every match of atoms [Verma et al., 2016a].

Overall the movement of atoms along each eigenvector showed the direction of motion of the protein. Trajectory files of MD simulations were utilized to portray the movement of native and mutant protein structures concentrating on the Cα atoms. gmx covar tool was used to obtain a set of eigenvectors and their respective eigenvalues as well as for diagonalization of matrix. gmx anaeig tool was used for analysis and plotting of the eigenvectors.

Results and discussion

In this study, we have analyzed the effect of mutations W68R and W68G in PZase enzyme coded by *pnc*A gene causing PZA resistance. Various analyses were performed including binding pocket determination, shape complementarity computation, receptor-ligand interactions and molecular dynamics simulations using protein-ligand complex structures.

Binding pocket analysis

Binding pocket volume of PZase proteins was evaluated using CASTp server. It measured the substrate binding cavity of protein which may differ between wild and mutant proteins and state the outcome of mutation. Significant difference was observed in the volume of native and mutant protein pockets. Binding pocket volume of native, mutant W68G and W68R was 504.9Å^3, 760.1Å^3 and 788.5 Å^3, respectively (Table1). The cavity volume for native protein was optimum for ligand binding. Increase or decrease in the cavity volume affected ligand occupancy. Increase in binding pocket volume of mutants indicated their role in altering significant protein side chain interaction with the drug.

Complementarity analysis

PatchDock web server estimated shape complementarity by calculating the docking score between receptor and ligand. The docking score obtained for PZA with native and mutants W68G & W68R complexes was 2686, 2254, and 2168, respectively (Table1). Shape complementarity between receptor and ligand indicated towards the strength of atomic interactions. Higher docking score for native protein stated higher magnitude of geometric complementarity for native protein and drug in comparison to the mutant forms.

Estimation of interaction energy between receptor and ligand molecules

Interaction energy of ligand-receptor complex is critical to comprehend the biological function of ligand molecule. Prior studies on PZase suggested that van der Waals forces were significant for ligand binding. Van der Waals forces and electrostatic interaction forces of protein-drug complexes were measured by Glide module of Schrodinger. Van der Waals forces and electrostatic forces showed higher complementarity between the native PZase and PZA molecules in comparison to the mutants (Table 1). Comparison of the native and mutant protein total interaction energies with PZA and complementarity analysis signified the characteristic difference of binding between the native and mutant protein-drug complexes. The docking score for native PZase protein was -4.069 while for mutant W68R and W68G was -3.973 and -3.175, respectively (Table 1). This showed that the PZA-PZase binding affinity for W68G mutant is significantly low and hence W68G mutant protein has less stable binding with PZA than W68R mutant or native PZase protein. . Thus, the overall deviation in the binding of ligand to receptor was due to the deforming mutations present in the active site of PZase protein.

Molecular dynamics trajectory analysis of protein and drug complexes

To understand the effect of mutations on the PZase structure and function, MD simulations were performed using the native and mutant proteins in complex with PZA drug. High performance molecular dynamics simulations of the protein-ligand complexes were performed for 40 ns. Various analyses were performed on the resultant trajectories. RMSD of backbone, RMSF of protein residues, Rg of complex, SASA of protein and hbond between the protein and ligand were investigated and compared for native and mutant proteins.

Root-mean-square deviations (RMSD) for backbone of the proteins was estimated which showed least deviation for native protein in comparison to the mutant structures W68G and W68R (Figure 1). Native structure showed deviations and achieved 0.23 nm of RMSD at ~6 ns. W68G structure achieved 0.25 nm of RMSD at ~10 ns and showed more deviations whereas W68R structure attained 0.35 nm at ~12 nm showed maximum deviation. From 22 ns to 40 ns, native structure was stable and maintained 0.25nm of backbone of RMSD with least deviations. W68G was stable from 22 ns to40 ns with a 0.26 nm of backbone of RMSD whereas W68R was stable with 0.33 nm RMSD. RMSD values of native and mutant proteins were stable after ~ 22 ns and showed similar fashion of deviation. MD trajectories reached convergence as plateau was

obtained within the time period of 22-40 ns (Figure 1). The trajectories obtained were stable and reliable and hence could be used for further analysis.

Potential energy of all protein complexes were calculated which revealed the potential energy of mutant protein complexes was higher than the native protein complex (Figure 2). This showed that the native protein complex was highly stable. Mutant W68R protein complex had a more positive value than native. Mutant W68G protein complex had the most positive value and is not stable. Like the RMSD values indicate, native protein is stably folded without any deviations whereas the mutant proteins showed reduced stability during the course of molecular dynamics.

Root-mean-square fluctuation (RMSF) was calculated for every residue of the native and mutant proteins. It can be observed that major fluctuations arose in the residues 51 to 104 (Figure 3). Fluctuations in mutant proteins were higher than occurring in the native protein. Native protein showed fluctuations ranging from 0.05 to 0.30 nm whereas W68G and W68R showed fluctuations ranging from 0.06 to 0.48 nm and 0.05 to 0.43 nm respectively. A higher RMSF value indicated high flexibility in the region whereas a low RMSF indicated constrained regions. There was higher flexibility in the residues 51 to 104 for the mutant proteins which imparted greater mobility to the amino acids forming a loosely packed protein throughout the MD simulation period which might have contributed to the lower affinity with the drug, PZA. The residues involved in the catalytic site and metal ion binding site showed major variations along with the active site residues. The catalytic triad Asp 8, Lys 96 and Cys 138 showed variations in the mutant W68G protein. On the other hand, the metal ion binding sites Asp 49, His 51, His57 and His71 showed major variations for both the mutant proteins W68G and W68R. The conserved regions of amino acids 61 to 85 showed major fluctuations ranging from 0.1 to 0.47 nm. The loop region, 52 to 70, which constituted the flap closing the binding cavity for PZA, showed higher fluctuations for the mutant proteins. Trp 68 is a part of the catalytic cleft which formed direct hydrogen bond with His 57. Mutation at this site had affected the proper positioning of PZA at the binding site in the protein. Fluctuations in the RMSF values proved the same.

Rg, radius of gyration was outlined as root mean-square distance of a cluster of atoms based on mass to weight ratio from the same center of mass. Rg was plotted against time which defines the

degree of compactness for protein during MD simulations (Figure 4). A stable Rg value signifies that there is no change in protein folding while varying values signify protein folding or unfolding. The plot obtained in case of native protein maintained stability through the simulation period, while mutant protein W68G showed highest variations. Mutant protein was less compact due to the mutations resulting in lower stability. Solvent accessible surface area (SASA) estimated the protein surface in contact with the solvent molecules. The solvation effect is important for maintaining the stability of protein and its structure. SASA was estimated using gmx sasa module for a simulation period of 40,000ps (Figure 5). SASA for the native protein was in the range from ~94 nm^2 to ~75 nm^2. The mutant W68R had SASA of ~95 nm^2 to ~77 $nm^2$and for the mutant W68G it was ~ 95 nm^2 to ~78 nm^2. Thus, there was not much of a difference in the solvent accessible surface of the native and mutant proteins.

NH bond analysis was done to comprehend the stability of the protein-ligand complex. Hydrogen bonds play a significant role in imparting stability to the protein structure. H-bonds between the protein and ligand molecule were analyzed during the 40 ns simulation period. Simulation of the protein complexes showed significant difference in the H-bonds formed between the proteins and ligand. H-bonds for the native as well as mutant protein-ligand structures were mostly 2 to 3 throughout the simulation (Figure 6).

Receptor-ligand interaction analysis

Hydrogen and hydrophobic interactions are important to maintain the proper functioning of protein-ligand complex. Hydrogen bonds and hydrophobic interactions were estimated for protein-ligand complexes after docking and MD simulation. Interaction plots were generated using Maestro and CHIMERA [Huang et al., 1996]

Native protein formed two H-bonds with PZA for which nitrogen atom of His137 and Cys138 were involved with oxygen atom of PZA having bond length of 2.50Å and 2.76Å, respectively (Fig 7). Mutant W68R also formed two H-bonds with PZA by Ala134 with bond length of 2.83Å and Cys 138 with bond length of 2.88Å (Fig 8). Mutant W68G formed two H-bonds with PZA. Oxygen atoms of Ser59 and Ser66 formed H-bond with nitrogen atom of PZA having bond length of 3.21Å and 2.93Å, respectively (Fig 9). There was a significant increase in the bond lengths of H-bond in the mutant proteins. This could be due to the increased binding pocket volume and highly rigid and non-flexible structure.

PZA showed hydrophobic interactions with Phe13, Asp49, His57 Phe58, Trp68, His71, Tyr103, Ala134, Asp136, and Val163 of native protein. PZA formed hydrophobic bonds with Asp8, Phe13, Leu19, Val21, Phe58, Ser66, Ser67, Ile133, His137, Val139, and Val163 of W68Rprotein whereas the residues Leu19, Asp56, His57, Phe58, Ser65, Tyr64, Ser67, Gly68, Tyr103, and Val163 were involved for mutant W68G protein. An overall increased number of hydrophobic bonds were observed between the mutant proteins and ligand. The binding interactions between PZA and PZase proteins have been listed in Table 2.

Essential dynamics analysis

Essential dynamics analysis was performed on the MD trajectory to study the changes in the motion between the proteins. Large-scale collective movements of the protein structures were estimated and dynamics of the proteins was obtained by characterization of their phase-space behavior. Figure 10 shows the overall secondary structural features of pyrazinamidase protein. Analysis of backbone atoms showed that the mutant proteins have less correlation in comparison to the native form (Figure 11). The red regions are the positive regions associated with the correlated residue movement in the same direction whereas the blue region is the negative region indicating anti-correlated residue motions in the opposite direction.

Residues of native protein-ligand complex found in correlated motions were: β-strand 3 and α-helix 1, α-helix 3 and α-helix 4. Anti-correlated motions were observed between β-strand 1 and α-helix 4, α-helix 3 and 3/10-helix, α-helix 4 and 3/10-helix, β-strand 3 and 3/10-helix. All these motions are important for optimal interaction between the protein and ligand, so that the protein can effectively act on the ligand. The mutant W68Rprotein-ligand complex residues showed correlated motions mostly similar to the native protein-ligand complex. The uncorrelated motions were in α-helix 3 and 3/10-helix, α-helix 4 and 3/10-helix, β-strand 3 and 3/10-helix and α-helix 1 and3/10-helix. The mutant W68G protein-ligand complex residues showed correlated motions same as the native protein-ligand complex. The uncorrelated motions were in α-helix 3 and 3/10-helix, α-helix 4 and 3/10-helix, and β-strand 3 and 3/10-helix.

Projection of proteins' motion was given by eigenvectors 1 and 2, eigenvectors 2 and 3, and eigenvectors 7 and 8 from each of the MD trajectory obtained as seen in Figure 12. The

corresponding eigenvalues indicated that variations in the protein system were restricted to first three eigenvectors and the proteins attained their equilibrium fluctuations within 8 eigenvectors. Analysis of these plots revealed that mutant W68R and W68G spread over a greater area of phase space than native protein mainly along PC1, PC2 and PC3 planes. It can thus be implied that the mutant proteins are more flexible than native protein at 310 K and tend to have more conformational fluctuations. Projection of the trajectories along the seventh and eighth principal components (PC7, PC8) was well defined for all the three native and mutant proteins. Hence, the three well defined trajectory clusters as shown in figure indicated the changes of conformational motion that occurred upon point mutation in the protein structure.

Conclusion

Due to increasing emergence of drug-resistant Mtb strains, present conventional therapies are rendered ineffective. Understanding the effect of gene mutation on structure of protein and its affinity for the ligand is required to aid the knowledge of drug development. This study is based on comprehensive analysis of the PZA drug resistance in *Mycobacterium tuberculosis* due to *pnc*A gene mutations. Binding pocket determination, shape complementarity computation, molecular docking, molecular dynamics simulation and essential dynamic studies have been performed. Docking of the native protein showed best complementarity between the receptor and ligand. The protein trajectories showed that there was increased flexibility in the mutant protein atoms. The mutant proteins were loosely packed, less compact and show lower stability. All the analyses showed that the protein had lost its compactness and stability because of the mutation. The H-bond and hydrophobic interactions between the receptor and ligand were different for the native and mutant proteins affecting the protein-drug interaction. The mutant W68G protein was found to drastically affect the structure of binding site of protein. The protein-drug interaction was inefficient due to the structural change resulting in PZA drug resistance in *Mycobacterium tuberculosis*. Mutation in the 68^{th} residue led to a structural change in the binding site of protein, thus PZA was not converted to its active form that renders it ineffective for TB treatment. The investigation of the dynamic behavior gave highly reliable information on the PZase mutation

affecting its structure and insights into the change in protein–ligand interactions due to conformational variations.

Acknowledgements

AG is thankful to Jawaharlal Nehru University for usage of all computational facilities. AG is grateful to University Grants Commission, India for the Faculty Recharge position.

Competing financial interests

Authors declare no competing financial interests.

References

Abraham MJ, Murtola T, Schulz R, Páll S, Smith JC, Hess B, Lindahl E. 2015. GROMACS: High performance molecular simulations through multi-level parallelism from laptops to supercomputers. SoftwareX 1:19-25.

Amadei A, Linssen A, Berendsen HJ. 1993. Essential dynamics of proteins. Proteins: Struct, Funct, Bioinf 17:412-425.

Bamaga M, Wright D, Zhang H. 2002. Selection of in vitro mutants of pyrazinamide-resistant Mycobacterium tuberculosis. Int J Antimicrob Agents 20:275-281.

Berendsen HJ, Postma Jv, van Gunsteren WF, DiNola A, Haak J. 1984. Molecular dynamics with coupling to an external bath. J Chem Phys 81:3684-3690.

Berendsen HJ, van der Spoel D, van Drunen R. 1995. GROMACS: a message-passing parallel molecular dynamics implementation. Comput Phys Commun 91:43-56.

Berman HM, Westbrook J, Feng Z, Gilliland G, Bhat T, Weissig H, Shindyalov IN, Bourne PE. 2000. The protein data bank. Nucleic Acids Res 28:235-242.

Chan RC, Hui M, Chan EW, Au T, Chin ML, Yip CK, AuYeang CK, Yeung CY, Kam KM, Yip PC. 2007. Genetic and phenotypic characterization of drug-resistant Mycobacterium tuberculosis isolates in Hong Kong. J Antimicrob Chemother 59:866-873.

Chang KC, Yew WW, Zhang Y. 2011. Pyrazinamide susceptibility testing in Mycobacterium tuberculosis: a systematic review with meta-analyses. Antimicrob Agents Chemother 55:4499-4505.

Cheng S-J, Thibert L, Sanchez T, Heifets L, Zhang Y. 2000. pncA mutations as a major mechanism of pyrazinamide resistance in Mycobacterium tuberculosis: spread of a monoresistant strain in Quebec, Canada. Antimicrob Agents Chemother 44:528-532.

Cole S, Brosch R, Parkhill J, Garnier T, Churcher C, Harris D, Gordon S, Eiglmeier K, Gas S, Barry Cr. 1998. Deciphering the biology of Mycobacterium tuberculosis from the complete genome sequence. Nature 393:537-544.

Da Silva PEA, Palomino JC. 2011. Molecular basis and mechanisms of drug resistance in Mycobacterium tuberculosis: classical and new drugs. J Antimicrob Chemother 66:1417-1430.

Darden T, York D, Pedersen L. 1993. Particle mesh Ewald: An N· log (N) method for Ewald sums in large systems. J Chem Phys 98:10089-10092.

Dooley KE, Mitnick CD, DeGroote MA, Obuku E, Belitsky V, Hamilton CD, Makhene M, Shah S, Brust JC, Durakovic N. 2012. Old drugs, new purpose: retooling existing drugs for optimized treatment of resistant tuberculosis. Clin. Infect. Dis. 55:572-581.

Du X, Wang W, Kim R, Yakota H, Nguyen H, Kim S-H. 2001. Crystal structure and mechanism of catalysis of a pyrazinamidase from Pyrococcus horikoshii. Biochemistry 40:14166-14172.

Duhovny D, Nussinov R, Wolfson HJ. 2002. Efficient unbound docking of rigid molecules. Algorithms in bioinformatics. Springer, p 185-200.

Dundas J, Ouyang Z, Tseng J, Binkowski A, Turpaz Y, Liang J. 2006. CASTp: computed atlas of surface topography of proteins with structural and topographical mapping of functionally annotated residues. Nucleic Acids Res 34:W116-W118.

Emekli U, Schneidman-Duhovny D, Wolfson HJ, Nussinov R, Haliloglu T. 2008. HingeProt: automated prediction of hinges in protein structures. Proteins: Struct, Funct, Bioinf 70:1219-1227.

Friesner RA, Banks JL, Murphy RB, Halgren TA, Klicic JJ, Mainz DT, Repasky MP, Knoll EH, Shelley M, Perry JK. 2004. Glide: a new approach for rapid, accurate docking and scoring. 1. Method and assessment of docking accuracy. J Med Chem 47:1739-1749.

Friesner RA, Murphy RB, Repasky MP, Frye LL, Greenwood JR, Halgren TA, Sanschagrin PC, Mainz DT. 2006. Extra precision glide: docking and scoring incorporating a model of hydrophobic enclosure for protein-ligand complexes. J Med Chem 49:6177-6196.

Glide V. 2009. 5.5, Schrodinger. New York, NY.

Gu Y, Yu X, Jiang G, Wang X, Ma Y, Li Y, Huang H. 2015. Pyrazinamide resistance among multidrug-resistant tuberculosis clinical isolates in a national referral center of China and its correlations with pncA, rpsA, and panD gene mutations. Diagn Microbiol Infect Dis.

Halgren TA, Murphy RB, Friesner RA, Beard HS, Frye LL, Pollard WT, Banks JL. 2004. Glide: a new approach for rapid, accurate docking and scoring. 2. Enrichment factors in database screening. J Med Chem 47:1750-1759.

Hess B, Bekker H, Berendsen HJ, Fraaije JG. 1997. LINCS: a linear constraint solver for molecular simulations. J Comput Chem 18:1463-1472.

Hess B, Kutzner C, Van Der Spoel D, Lindahl E. 2008. GROMACS 4: algorithms for highly efficient, load-balanced, and scalable molecular simulation. J Chem Theory Comput 4:435-447.

Huang CC, Couch GS, Pettersen EF, Ferrin TE. 1996. Chimera: an extensible molecular modeling application constructed using standard components. Pacific symposium on biocomputing. p 1519-1523.

Jamal S, Goyal S, Shanker A, Grover A. 2016. Integrating network, sequence and functional features using machine learning approaches towards identification of novel Alzheimer genes. BMC genomics 17:807.

Jones S, Thornton JM. 1996. Principles of protein-protein interactions. Proc Natl Acad Sci 93:13-20.

Kim S, Thiessen PA, Bolton EE, Chen J, Fu G, Gindulyte A, Han L, He J, He S, Shoemaker BA. 2015. PubChem substance and compound databases. Nucleic Acids Res:gkv951.

Konno K, Feldmann FM, McDermott W. 1967. Pyrazinamide Susceptibility and Amidase Activity of Tubercle Bacilli 1, 2. Am Rev Respir Dis 95:461-469.

Lakshmipathy D, Ramasubban G, Therese L, Vetrivel U, Sivashanmugam M, Rajendiran S, Sridhar R, Madhavan H, Meenakshi N. 2013. In silico Analysis of Novel Mutation ala102pro Targeting pncA Gene of M. Tuberculosis. J Comp Sci & Sys Biol 2013.

Lee KW, Lee JM, Jung KS. 2001. Characterization of pncA mutations of pyrazinamide-resistant Mycobacterium tuberculosis in Korea. J Korean Med Sci 16:537.

Lemaitre N, Sougakoff W, Truffot-Pernot C, Jarlier V. 1999. Characterization of New Mutations in Pyrazinamide-Resistant Strains of Mycobacterium tuberculosisand Identification of Conserved Regions Important for the Catalytic Activity of the Pyrazinamidase PncA. Antimicrob Agents Chemother 43:1761-1763.

Malone L, Schurr A, Lindh H, McKenzie D, Kiser J, Williams J. 1952. The Effect of Pyrazinamide (Aldinamide) on Experi-mental Tuberculosis in Mice. Am Rev Respir Dis 65:511-18.

McKenzie D, Malone L, Kushner S, Oleson J, Subbarow Y. 1948. The Effect of Nieotinic Acid Amide on Experimental Tuberculosis of White Mice. J Lab Clin Med 33:1249-53.

Mitchison D. 1985. The action of antituberculosis drugs in short-course chemotherapy. Tubercle 66:219-225.

Nagpal N, Goyal S, Wahi D, Jain R, Jamal S, Singh A, Rana P, Grover A. 2015. Molecular principles behind Boceprevir resistance due to mutations in hepatitis C NS3/4A protease. Gene 570:115-121.

Organization WH. 2015. Global tuberculosis report 2015.

Organization WH. 2016. Global tuberculosis report 2016.

Pandey B, Grover S, Tyagi C, Goyal S, Jamal S, Singh A, Kaur J, Grover A. 2016. Molecular principles behind pyrazinamide resistance due to mutations in panD gene in Mycobacterium tuberculosis. Gene 581:31-42.

Parrinello M, Rahman A. 1981. Polymorphic transitions in single crystals: A new molecular dynamics method. J Appl Phys 52:7182-7190.

Petrella S, Gelus-Ziental N, Maudry A, Laurans C, Boudjelloul R, Sougakoff W. 2011. Crystal structure of the pyrazinamidase of Mycobacterium tuberculosis: insights into natural and acquired resistance to pyrazinamide. PLoS One 6:e15785.

Purohit R, Rajendran V, Sethumadhavan R. 2011. Relationship between mutation of serine residue at 315th position in M. tuberculosis catalase-peroxidase enzyme and Isoniazid susceptibility: an in silico analysis. J Mol Model 17:869-877.

Release S. 2013. 2: LigPrep, version 2.7. Schrödinger, LLC, New York, NY.

Ryan F. 1993. The Forgotten Plague: How the battle against tuberculosis was won--and lost.

Sastry GM, Adzhigirey M, Day T, Annabhimoju R, Sherman W. 2013. Protein and ligand preparation: parameters, protocols, and influence on virtual screening enrichments. J Comput Aided Mol Des 27:221-234.

Schneidman-Duhovny D, Inbar Y, Nussinov R, Wolfson HJ. 2005. PatchDock and SymmDock: servers for rigid and symmetric docking. Nucleic Acids Res 33:W363-W367.

Schrödinger L. The PyMOL Molecular Graphics System. 1.4.: Schrödinger: LLC.

Schrödinger L. 2013. Schrödinger Suite 2011 Protein Preparation Wizard. Epik version 2.

SchuÈttelkopf AW, Van Aalten DM. 2004. PRODRG: a tool for high-throughput crystallography of protein–ligand complexes. Acta Crystallogr D Biol Crystallogr 60:1355-1363.

Scorpio A, Lindholm-Levy P, Heifets L, Gilman R, Siddiqi S, Cynamon M, Zhang Y. 1997. Characterization of pncA mutations in pyrazinamide-resistant Mycobacterium tuberculosis. Antimicrob Agents Chemother 41:540-543.

Scorpio A, Zhang Y. 1996. Mutations in pncA, a gene encoding pyrazinamidase/nicotinamidase, cause resistance to the antituberculous drug pyrazinamide in tubercle bacillus. Nat Med 2:662-667.

Sheen P, Ferrer P, Gilman RH, Christiansen G, Moreno-Román P, Gutiérrez AH, Sotelo J, Evangelista W, Fuentes P, Rueda D. 2012. Role of metal ions on the activity of Mycobacterium tuberculosis pyrazinamidase. Am J Trop Med Hyg 87:153-161.

Shi W, Zhang X, Jiang X, Yuan H, Lee JS, Barry CE, Wang H, Zhang W, Zhang Y. 2011. Pyrazinamide inhibits trans-translation in Mycobacterium tuberculosis. Science 333:1630-1632.

Singh A, Goyal S, Jamal S, Subramani B, Das M, Admane N, Grover A. 2016. Computational identification of novel piperidine derivatives as potential HDM2 inhibitors designed by fragment-based QSAR, molecular docking and molecular dynamics simulations. Struct Chem 27:993-1003.

Singh A, Grover S, Sinha S, Das M, Somvanshi P, Grover A. 2017. Mechanistic principles behind molecular mechanism of Rifampicin resistance in mutant RNA polymerase beta subunit of Mycobacterium tuberculosis. J Cell Biochem.

Sinha S, Tyagi C, Goyal S, Jamal S, Somvanshi P, Grover A. 2016. Fragment based G-QSAR and molecular dynamics based mechanistic simulations into hydroxamic-based HDAC inhibitors against spinocerebellar ataxia. J Biomol Struct Dyn:1-15.

Solotorovsky M, Gregory F, Ironson E, Bugie E, O'Neill R, Pfister K. 1952. Pyrazinoic acid amide-An agent active against experimental murine tuberculosis. Exp Biol Med 79:563-565.

Stehr M, Elamin AA, Singh M. 2015. Pyrazinamide: the importance of uncovering the mechanisms of action in mycobacteria. Expert Rev Anti Infect Ther 13:593-603.

Unissa AN, Sudha S, Selvakumar N. 2011. Elucidating pyrazinamide resistance in mycobacterium tuberculosis by molecular docking.

Van Der Spoel D, Lindahl E, Hess B, Groenhof G, Mark AE, Berendsen HJ. 2005. GROMACS: fast, flexible, and free. J Comput Chem 26:1701-1718.

van Gunsteren WF, Billeter S, Eising A, Hünenberger PH, Krüger P, Mark AE, Scott W, Tironi IG. 1996. Biomolecular simulation: The {GROMOS96} manual and user guide.

Vats C, Dhanjal JK, Goyal S, Gupta A, Bharadvaja N, Grover A. 2015. Mechanistic analysis elucidating the relationship between Lys96 mutation in Mycobacterium tuberculosis pyrazinamidase enzyme and pyrazinamide susceptibility. BMC genomics 16:1.

Verma S, Goyal S, Tyagi C, Jamal S, Singh A, Grover A. 2016a. BIM (BCL-2 interacting mediator of cell death) SAHB (stabilized α helix of BCL2) not always convinces BAX (BCL-2-associated X protein) for apoptosis. J Mol Graph Model 67:94-101.

Verma S, Grover S, Tyagi C, Goyal S, Jamal S, Singh A, Grover A. 2016b. Hydrophobic Interactions Are a Key to MDM2 Inhibition by Polyphenols as Revealed by Molecular Dynamics Simulations and MM/PBSA Free Energy Calculations. PLoS One 11:e0149014.

Verma S, Tyagi C, Goyal S, Pandey B, Jamal S, Singh A, Grover A. 2016c. Mutations induce conformational changes in folliculin C-terminal domain: possible cause of loss of guanine exchange factor activity and Birt-Hogg-Dubé syndrome. J Biomol Struct Dyn:1-6.

Wu Y, Tepper HL, Voth GA. 2006. Flexible simple point-charge water model with improved liquid-state properties. J Chem Phys 124:024503.

Yeager R, Munroe W, Dessau FI. 1952. Pyrazinamide (aldinamide) in the treatment of pulmonary tuberculosis. American Review of Tuberculosis and Pulmonary Diseases 65:523-46.

Zhang C, Vasmatzis G, Cornette JL, DeLisi C. 1997. Determination of atomic desolvation energies from the structures of crystallized proteins. J Mol Biol 267:707-726.

Zhang H, Deng JY, Bi LJ, Zhou YF, Zhang ZP, Zhang CG, Zhang Y, Zhang XE. 2008. Characterization of Mycobacterium tuberculosis nicotinamidase/pyrazinamidase. FEBS J 275:753-762.

Zhang S, Chen J, Shi W, Liu W, Zhang W, Zhang Y. 2013. Mutations in panD encoding aspartate decarboxylase are associated with pyrazinamide resistance in Mycobacterium tuberculosis. Emerg Microbes Infect 2:e34.

Zhang Y, Mitchison D. 2003. The curious characteristics of pyrazinamide: a review. Int J Tuberc Lung Dis 7:6-21.

Zhang Y, Scorpio A, Nikaido H, Sun Z. 1999. Role of acid pH and deficient efflux of pyrazinoic acid in unique susceptibility of Mycobacterium tuberculosis to pyrazinamide. J Bacteriol 181:2044-2049.

Zhang Y, Telenti A. 2000. Genetics of drug resistance in Mycobacterium tuberculosis. Molecular genetics of mycobacteria. ASM Press, Washington, DC.

Figure Legends

Figure 1: Root mean square deviation (backbone) as a function of time for native and mutant proteins bound to PZA.

Figure 2: Potential energy of the native and mutant proteins bound to PZA versus time.

Figure 3: Root-mean square fluctuation of all residues of native and mutant proteins bound to PZA.

Figure 4: Radius of gyration of Cα atoms of native and mutant proteins bound to PZA.

Figure 5: Solvent accessible surface area of the complex of native and mutant proteins bound to PZA.

Figure 6: Hydrogen bonds formed by the native and mutant protein with PZA.

Figure 7: PZA interaction with Native W68 PZase protein (A) Hydrogen bonds, (B) hydrophobic interactions.

Figure 8: PZA interaction with Mutant W68R PZase protein (A) Hydrogen bonds, (B) hydrophobic interactions.

Figure 9: PZA docking interaction with Mutant W68G PZase protein (A) Hydrogen bonds, (B) hydrophobic interactions.

Figure 10: PZase protein illustration of secondary structure elements: α-helix and β-strand and coordinated Fe atom.

Figure 11: Covariance matrix A. Native W68 protein, B. Mutant W68R protein, C. Mutant W68G protein.

Figure 12: Projection of the motion of the protein in phase space at 300K A. Along the principal eigenvectors 1 and 2, B. Along the principal eigenvectors 2 and 3, C. Along the principal eigenvectors 7 and 8.

Table 1: Binding pocket analysis showing total cavity volume , Shape complementarity analysis showing PatchDock score and Receptor-ligand interaction analysis showing interaction energies.

Enzyme	Binding pocket volume (Å^3)	PatchDock Score	Docking score	Ligand–receptor electrostatic energy (Kcal/mol)	Ligand–receptor van der Waals energy (Kcal/mol)	Total ligand–receptor interaction energy (Kcal/mol)
Native	504.9	2686	-4.069	-1028.96	-1579.79	-27.197916
Mutant W68G	760.1	2254	-3.175	-1008.47	-1583	-19.746727
Mutant W68R	788.5	2168	-3.973	-995.11	-1547.3	-22.116834

Table 2: Binding interactions between PZA and native and mutant PZase.

Protein	H-bond	Hydrophobic bond
NATIVE W68 protein-ligand complex	His137, Cys138	Phe13, Asp49, His57 Phe58, Trp68, His71, Tyr103, Ala134, Asp136, Val163
Mutant W68R protein-ligand complex	Ala134, Cys138	Asp8, Phe13, Leu19, Val21,Phe58, Ser66, Ser67, Ile133, His137, Val139, Val163
Mutant W68G protein-ligand complex	Ser59, Ser66	Leu19, Asp56, His57, Phe58, Ser65, Tyr64, Ser67, Gly68, Tyr103, Val163

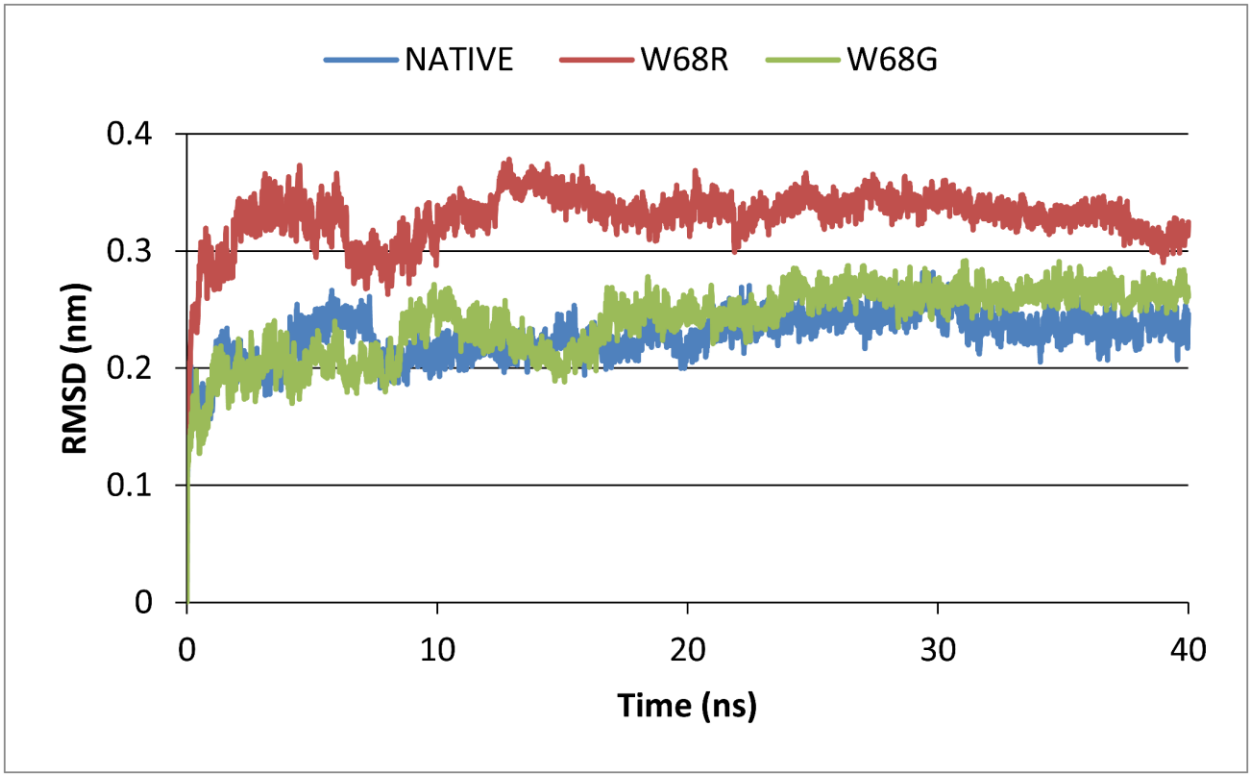

Figure 1

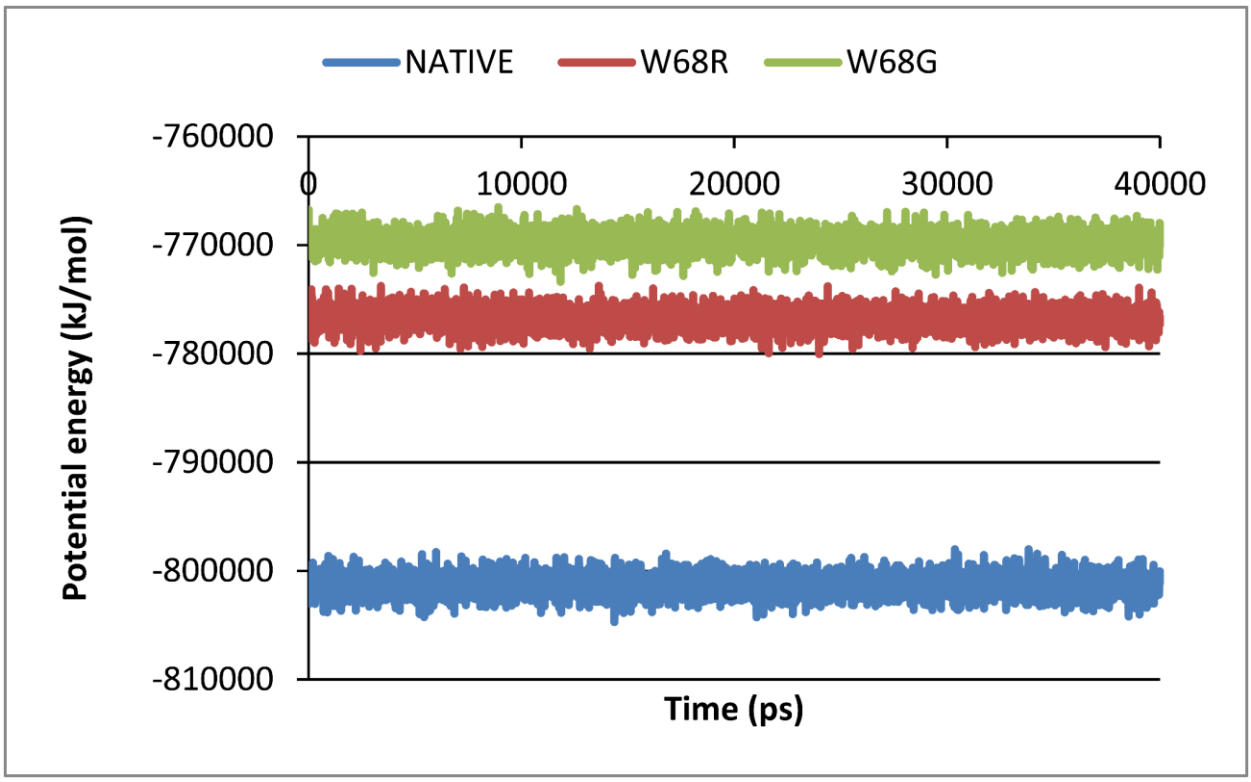

Figure 2

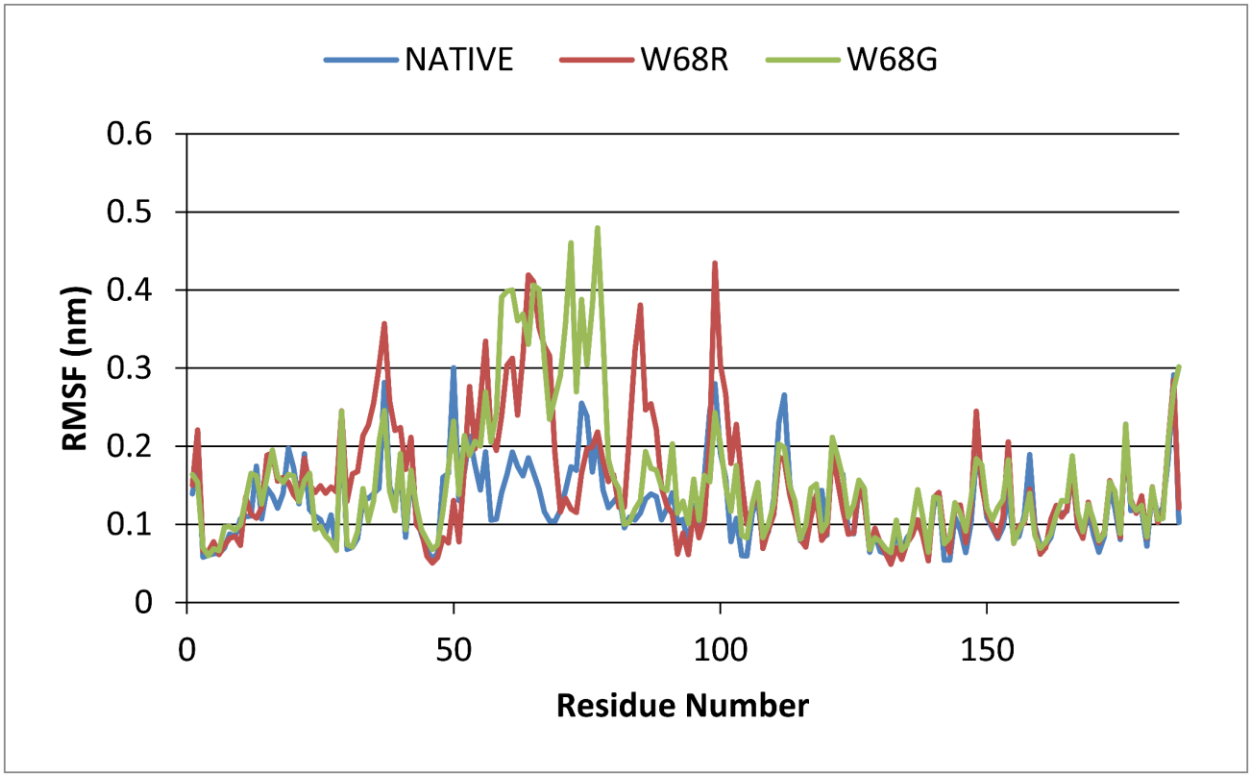

Figure 3

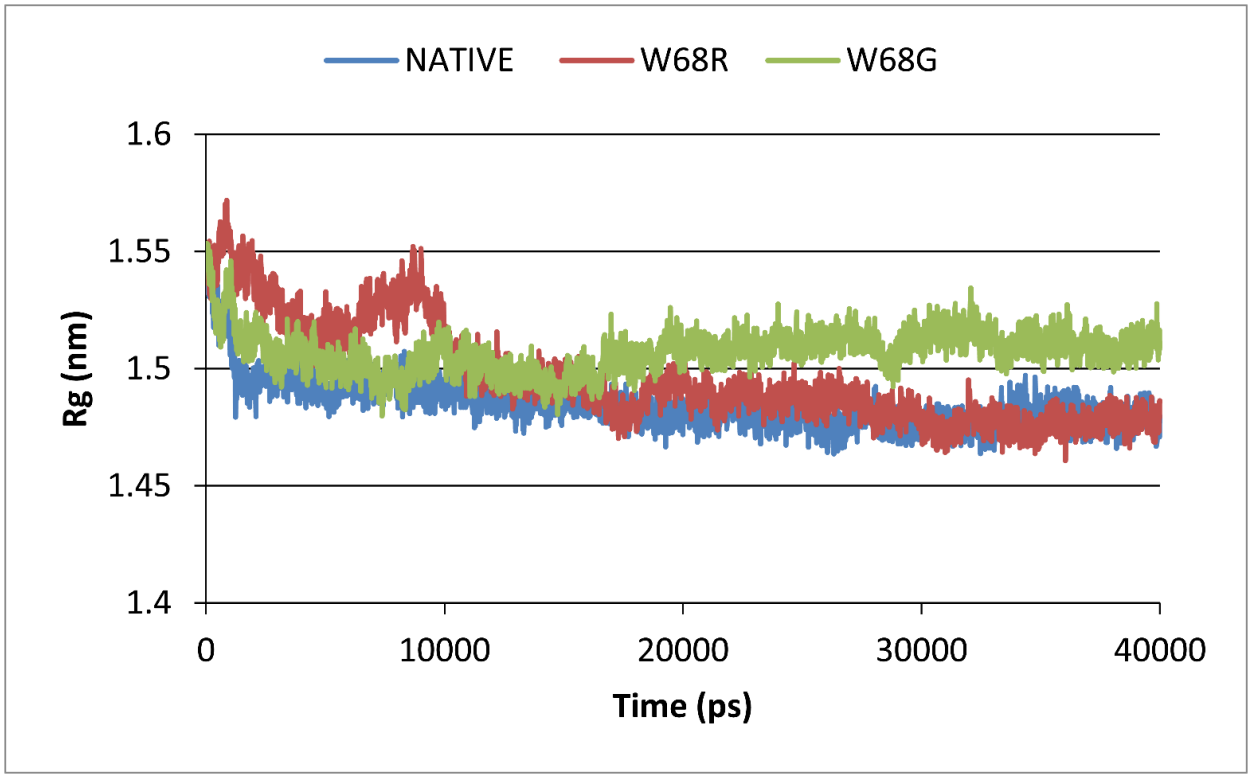

Figure 4

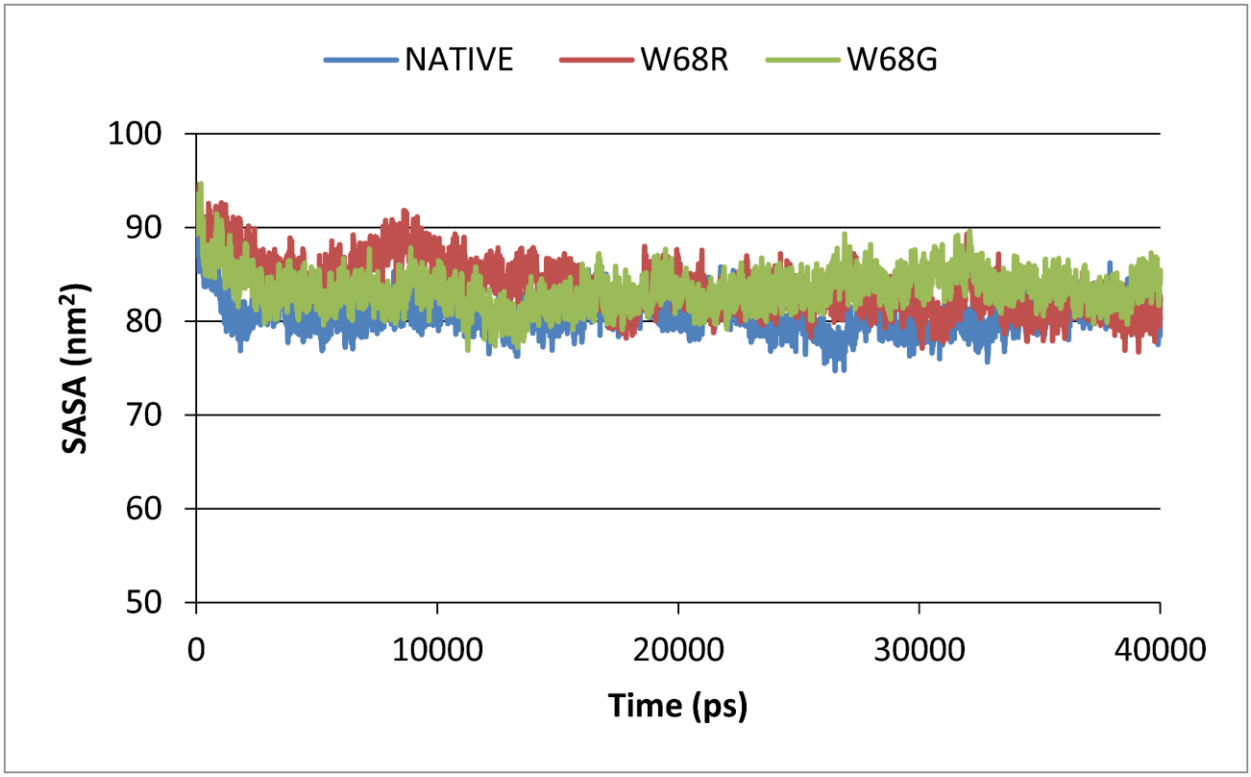

Figure 5

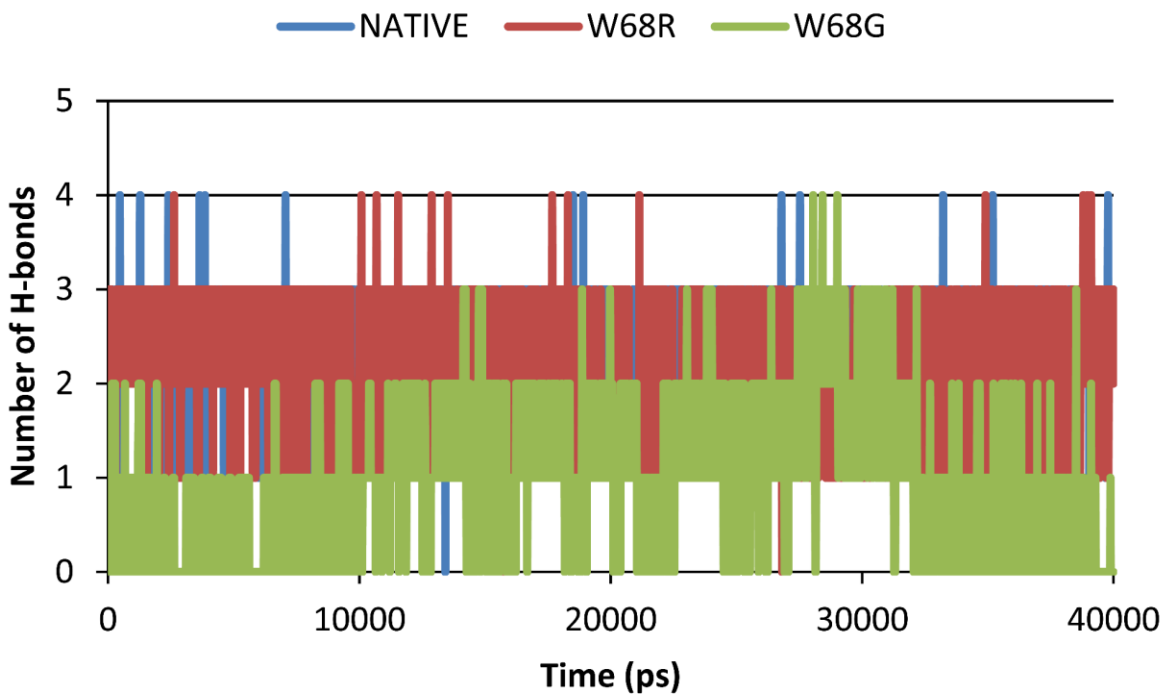

Figure 6

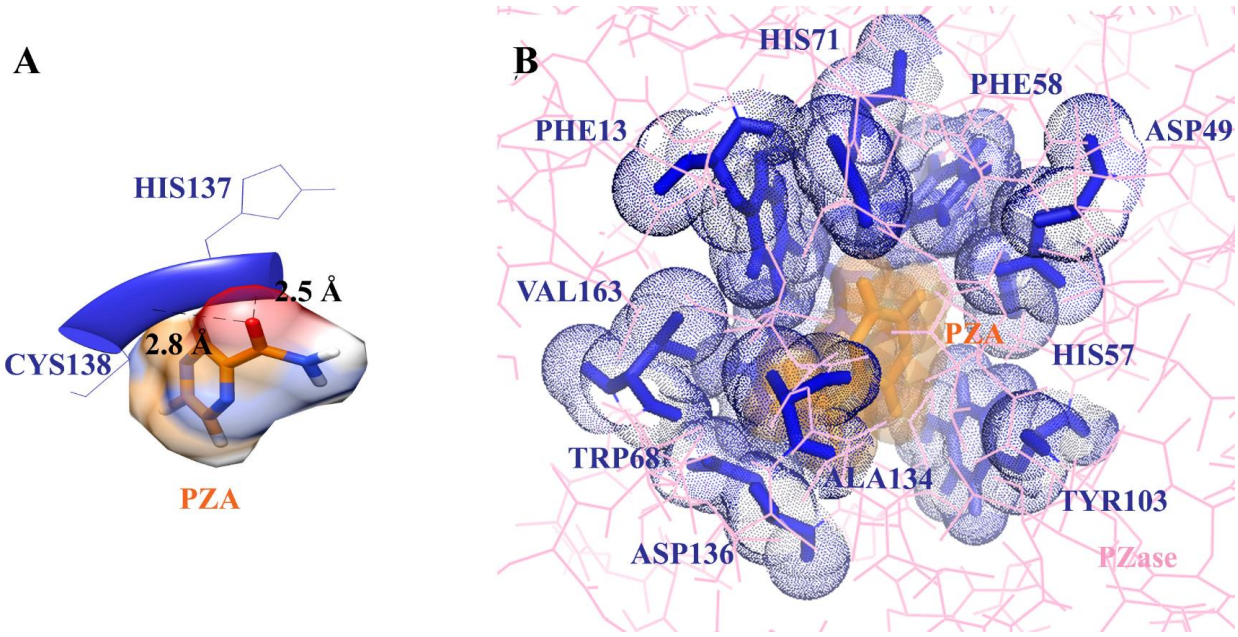

Figure 7

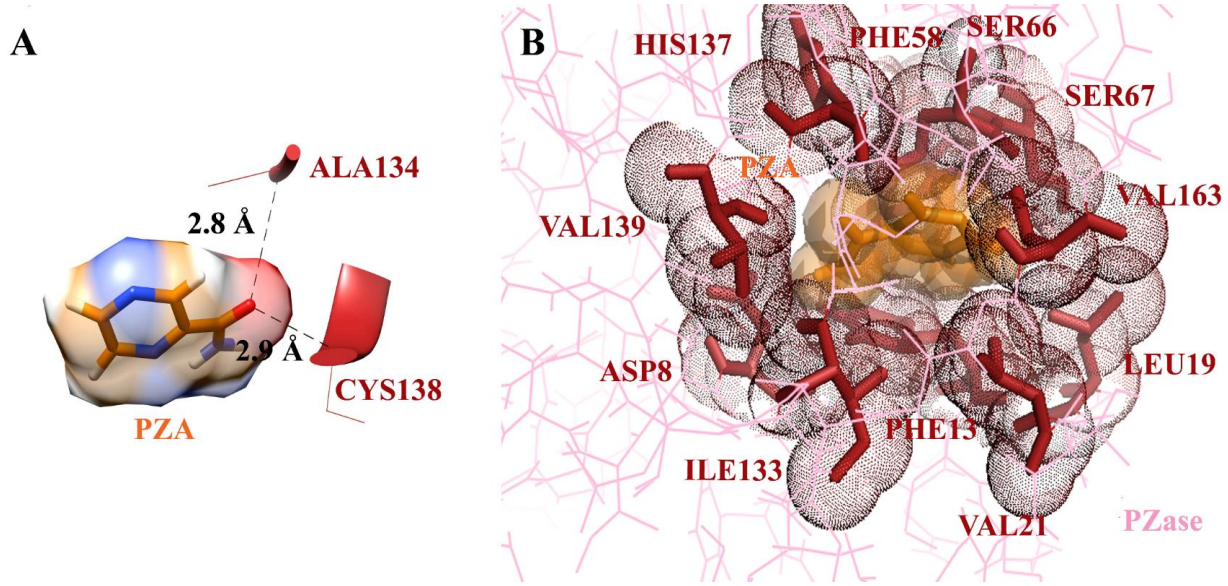

Figure 8

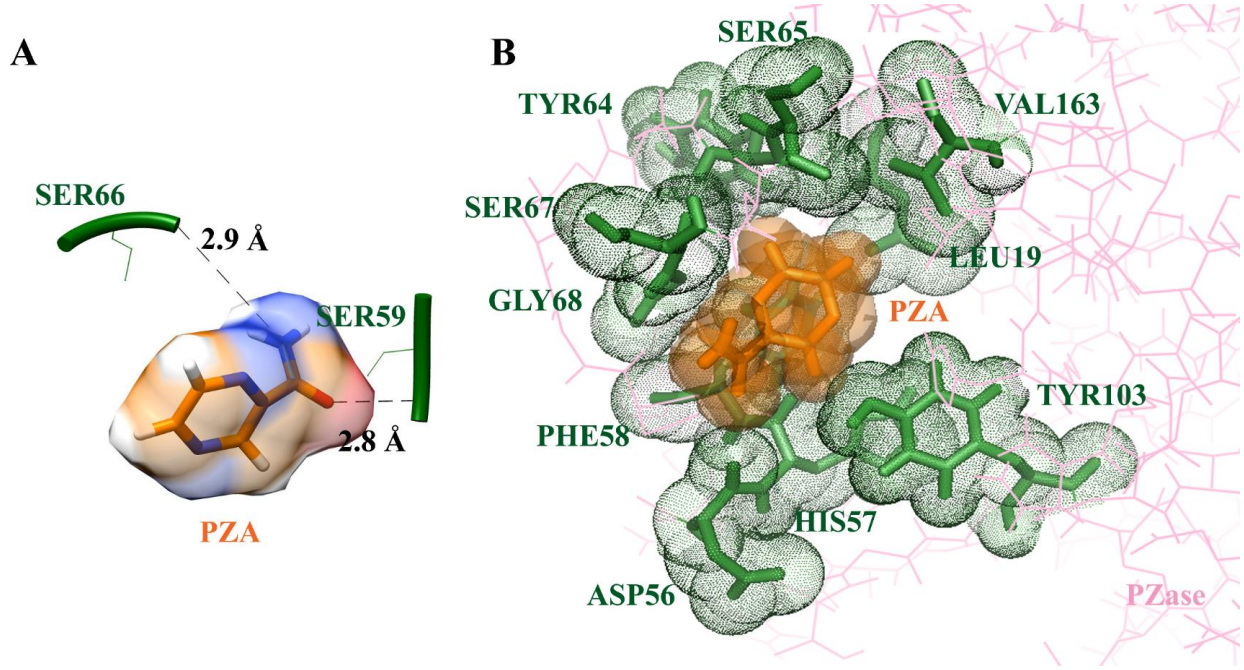

Figure 9

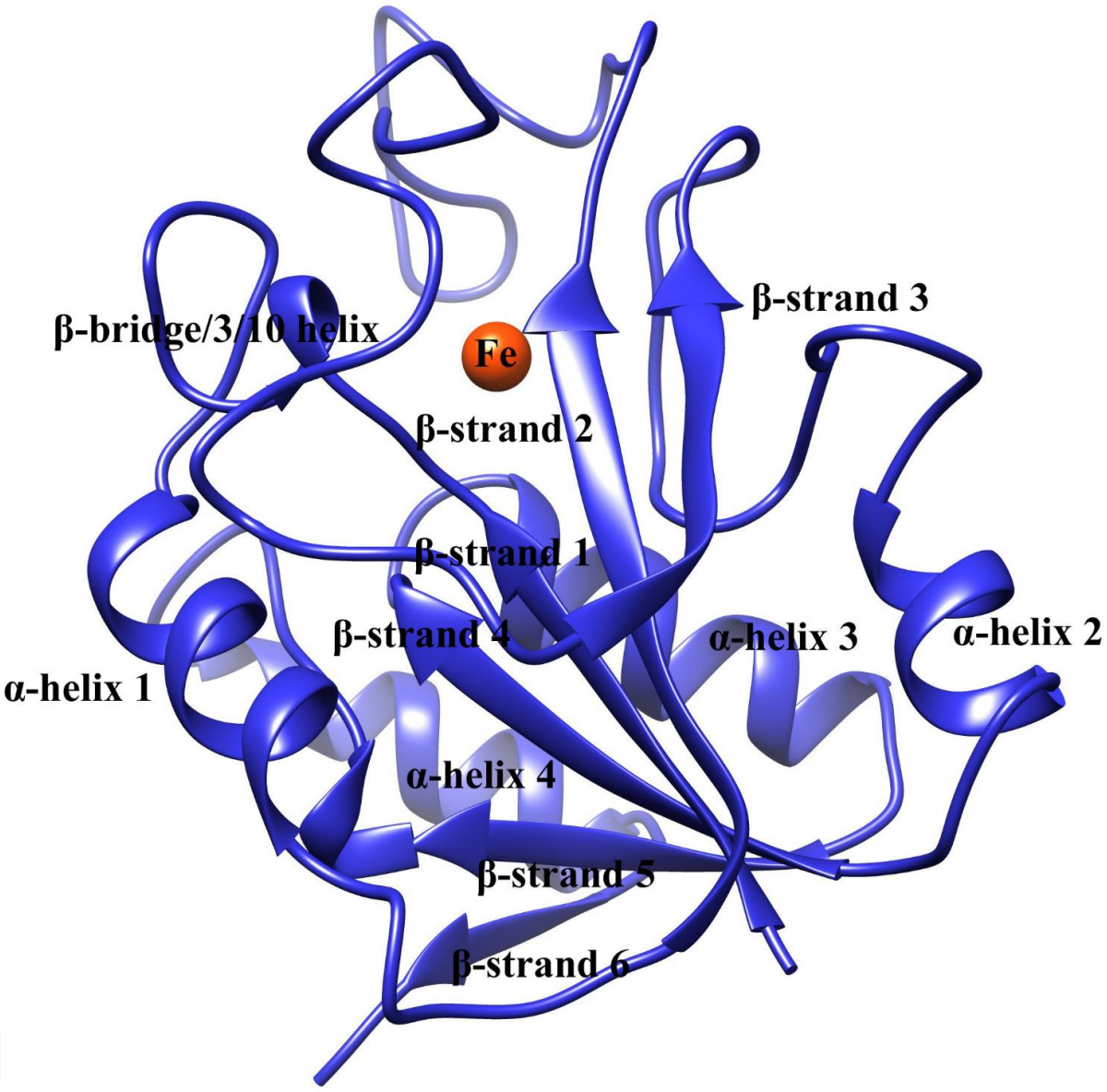

Figure 10

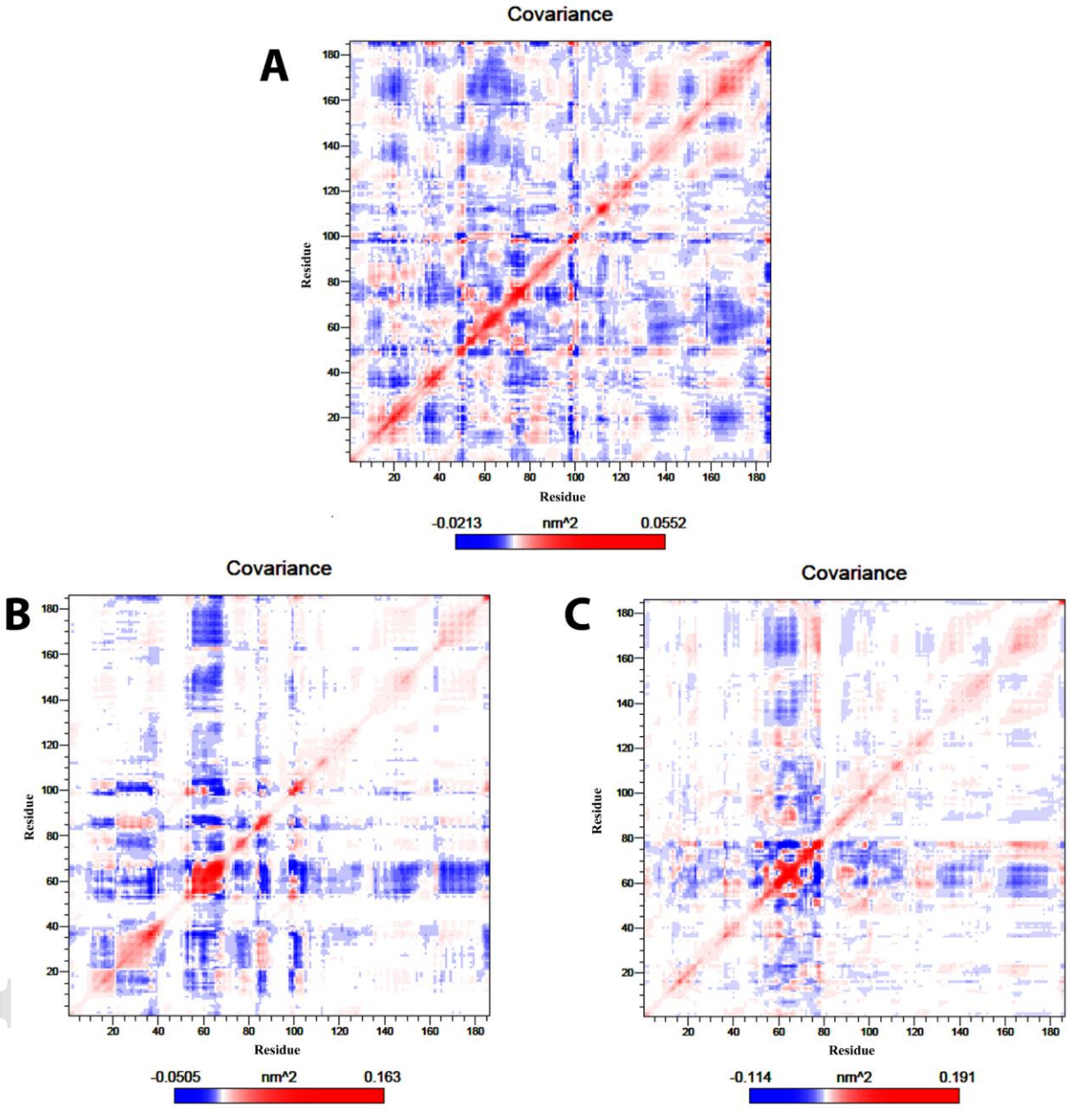

Residues 2-7 β-strand 1, 10-13 β-bridge/3/10-helix, 24-31 α-helix 1, 43-49 β-strand 2, 92-96 β-strand 3, 116-122 α-helix 2, 127-132 β-strand 4, 138-149 α-helix 3, 152-160 β-strand 5, 165-178 α-helix 4, 181-183 β-strand 6

Figure 11

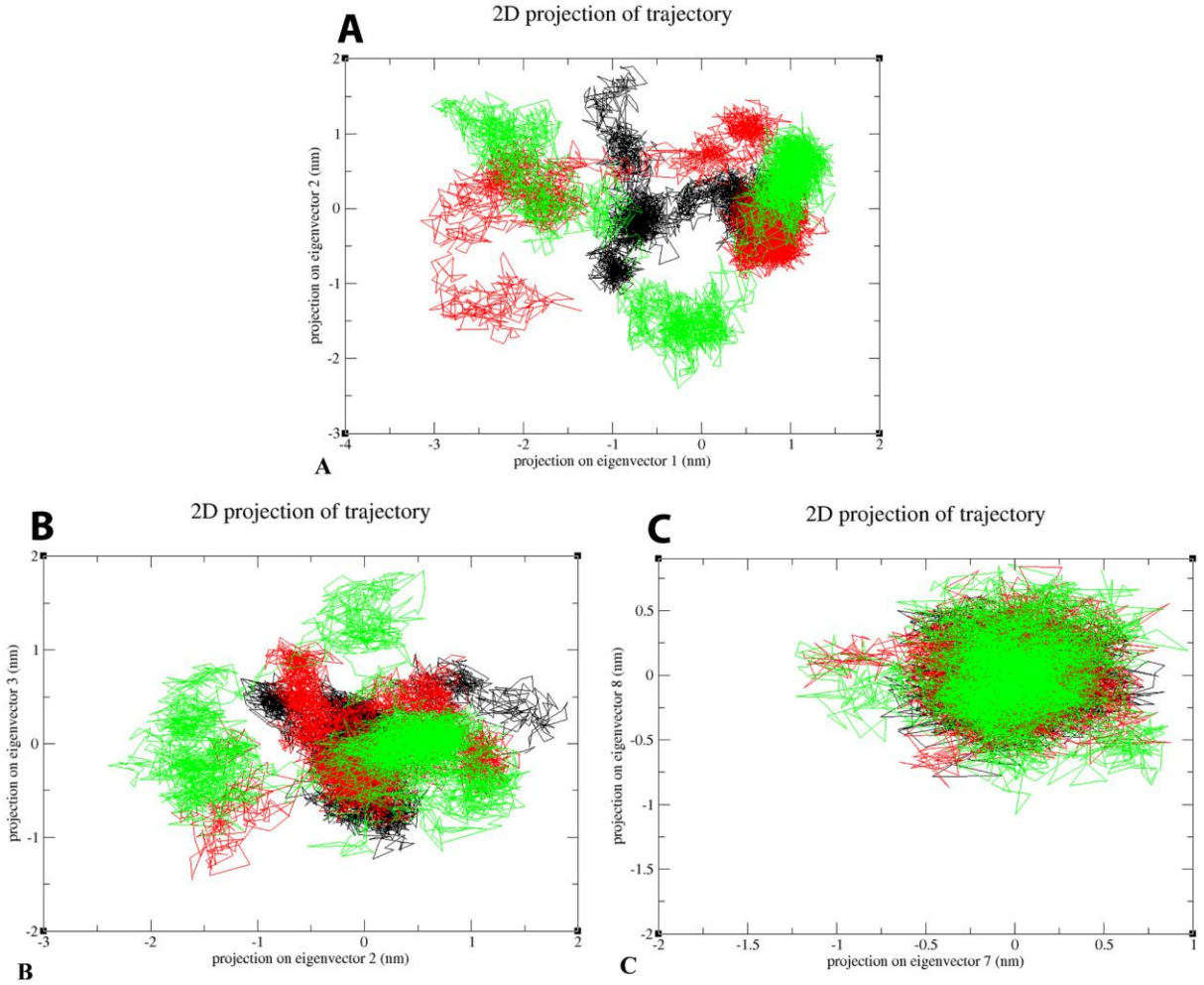

Figure 12